Hindawi
International Journal of Optics
Volume 2019, Article ID 2815890, 8 pages
https://doi.org/10.1155/2019/2815890

*Research Article*

# Effect Analysis of Optical Masking Algorithm for GEO Space Debris Detection

**Sijie Kong**,[1,2] **Jin Zhou**,[1] **and Wenli Ma**[1]

[1] *The Institute of Optics and Electronics, Chinese Academy of Science, Chengdu 610209, China*
[2] *University of Chinese Academy of Sciences, Beijing 100049, China*

Correspondence should be addressed to Wenli Ma; mawenli@ioe.ac.cn

Received 26 December 2018; Revised 11 February 2019; Accepted 19 February 2019; Published 26 March 2019

Academic Editor: Sulaiman W. Harun



A method with high detection rate, low false-alarm rate, and low computational cost is presented for removing stars and noise and detecting space debris with signal-to-noise ratio (SNR>3) in consecutive raw frames. The top-hat transformation is implemented firstly to remove background, then a masking technique is proposed to remove stars, and finally, a weighted algorithm is used to detect the pieces of space debris. The simulation samples are images taken by 600 mm ground-based telescope. And a series of simulation targets are added to the image in order to test the detection rate and false-alarm rate of different SNRs. The telescope in this paper is worked in "staring target mode." The experimental results show that the proposed method can detect space debris effectively with low false-alarm by only three frames. When the SNR is higher than 3, the detection probability can reach 94%, and the false-alarm rate is below 2%. The running time of this algorithm is within 1 second. Additionally, algorithm performance tests in different regions are also carried out. A large set of image sequences are tested, which proves the stableness and effectiveness of the proposed method.

## 1. Introduction

Space debris refers to the man-made nonfunctional object of all sizes in near-earth space, which has been produced since the first launch of the artificial Earth satellite [1]. Space debris includes defunct satellites, paint flakes, and solid rocket motor slag as well as debris created by explosions and collisions. Furthermore, it is mostly found in orbits with altitudes ranging from 300 to 400,000 km, posing a major risk to current and future space mission. As of April 2015, more than 17,000 space objects, larger than 10 cm, have been cataloged, among which only 6% are normally operating spacecraft. The number of space debris larger than 1 cm is 500 thousand, and that larger than 1mm is 35 million. Space debris is not invariant in space, but rolling and moving with light and orbit changing all the time. In addition, it is colliding and breaking down ceaselessly, thus producing new debris. Due to these characteristics, space debris is difficult to be searched and detected.

In Low Earth Orbit (LEO) region, most of the objects larger than 20 cm have been cataloged, as the objects in this region can be detected by both radar measurements and optical measurements. However, debris in Geosynchronous Earth Orbit (GEO), which is smaller and fainter, has been investigated less adequately [2], since it can only be detected by optical measurements, like optical telescopes with large aperture and wide-field view. The acquisition of objects trajectories relies on wide-field view observations, object detection, global stations, and trajectory extractions, among which object detection is extremely important and crucial.

The processing steps of space debris survey involve the algorithms of detecting objects, determining orbits, estimating physical size, and eventually cataloging objects. In terms of challenges, debris detection faces small and dim target, a large number of stellar background interference, and a large amount of data processing. Various algorithms have been developed to detect dim and small objects, such as maximum likelihood ratio [3], three-dimensional matched filtering [4–6], and dynamic programming algorithm [7, 8]. Despite the effectiveness of these algorithms in detecting dim and small objects in image sequences, they fail to remove background stars completely. Therefore, a more effective

algorithm applicable to the star background is of significance to object detection.

In engineering practice, traditional subtraction technique has been widely used, because of its simple calculation and short processing time. Subtraction technique is a method of eliminating stellar interference and highlighting target signal through interframe difference [9]. By contrast, a variety of stars that seem similar to space debris are flickering and undulating between different frames, and these stars cannot be entirely removed after frame subtraction. Thus, in the subtraction technique, usually four to six frames are needed for the calculation and removal of the star background. Thomas Schildknecht has proposed a masking technique [10–13], in which a template frame (also called mask) is employed to mask all background stars on the search frames1. This method has been successfully applied to the Zimmerwald 1-m ZIMLAT telescope, which tracks space debris with its expected motion during the exposure and is repositioned between the exposures in order to observe the same field in the sky all the time [1]. Nevertheless, the way of moving telescope is not suitable for our large telescope, owing to the jitter error produced by back and forth movement of telescope. Sun has put forward a detection pipeline through median filtering and mathematical morphology [14], in which six frames are employed to extract objects, and the detection ability for faint objects is improved. Moreover, both detection accuracy and detection efficiency are important to the space debris detection system. In this paper, a new technology is proposed to achieve the extraction of objects (SNR>3) by three frames, with the detection probability above 94% and the false-alarm rate below 2%.

In this paper, a space debris detection method is proposed using a masking technique for the removal of stars and a weighted algorithm for the correction of spurious detection. Only three frames are needed in the detection of space debris. The survey techniques for space debris in GEO are generally introduced in Section 2. In Section 3, the results of application are provided and the discussions are made. Finally, the conclusion is drawn in Section 4.

## 2. Theories

The so-called high-altitude class of earth orbits is the orbits with apogees at altitudes higher than 2000 km. A variety of orbit families exist in this class, including the most famous geostationary earth orbit (GEO) at 36000 km altitudes. The GEO (Geosynchronous Earth Orbit) region usually used by communication satellites like television broadcast is a circular orbit with an inclination of 0° in the equatorial plane. Space debris in this region is not moving relative to the earth. Because of the long distance between geostationary and ground, the space debris is too small and dim to detect.

The ground-based telescope used for GEO objects detection usually surveys in two methods. One is "staring star mode"; the other is staring target mode." In the former mode, the telescope moves synchronously with the star background during the exposure. After each exposure, the telescope is moved in a way that the same area of star background appears at the same field of view on the next exposure. In the latter mode, the telescope is in one direction during the exposure time and exposure gaps. Therefore, search frames of "staring star mode" from the ground-based telescope including point-like stars and streak-like objects. In contrast, search frames of "staring target mode" cover point-like objects and streak-like stars. In this paper, the telescope was worked in "staring target mode," as the space debris in geostationary ring is relatively stationary.

The optical image taken by ground-based telescope is modeled as [15]

$$f(i,j) = D(i,j) + S(i,j) + B(i,j) + n(i,j) \tag{1}$$

where $S(i, j)$ and $D(i, j)$ represent stars and space debris, respectively. $B(i, j)$ refers to background, which is nonuniform due to the effects of different CCD channels and the light conditions around the telescope. The noise $n(i, j)$ is generated by CCD dark current noise and space radiation.

The methodology used by the survey for space debris in GEO is outlined later. And its block diagram is llustrated in Figure 1. First, mathematical morphology was adopted in textcolorredthe background estimation and removal. As the images were detected by telescopes and the bright stars moved towards the specified direction and velocity, the stars overlapped on the media frame. Hence the masking technique was developed to remove bright stars. At last, based on the characteristics of the masking operator, a number of noise and star edges exist. Hence a binary segment and weighted calculation were adopted to reduce noise false alarm.

*2.1. Image Preprocessing.* For digital images taken by the telescope, there are many factors that cause the nonuniform background of the image, such as thin cloud, skylight conditions, and different CCD channels. Nonuniform background makes it difficult to segment objects from the background. In the beginning of the methodology, the mathematical morphology operator on the raw frames was adopted to remove the nonuniform background. Mathematical morphology transformation is composed of two basic operators: dilation and erosion. These two operators of a gray image $f(i, j)$ by structure element $b(x, y)$ are defined as

$$\begin{aligned}(f \oplus b)(i,j) = \min\{&f(i-x, j-y) \\ &+ b(x,y) \mid (i-x, j-y) \in D_f;\ (x,y) \in D_b\}\end{aligned} \tag{2}$$

$$\begin{aligned}(f \ominus b)(i,j) = \min\{&f(i+x, j+y) \\ &- b(x,y) \mid (i+x, j+y) \in D_f;\ (x,y) \in D_b\}\end{aligned} \tag{3}$$

$D_f$ and $D_b$ are domain of $f$ and $b$. The structure element $b$ is defined by the field of view of the telescope, the pattern of observations, and the size of the stars and space objects in the image. If the structural elements are too small, they will filter out stars and space targets. On the contrary, if the structural elements are too big, the uneven background of the image cannot be effectively filtered. Therefore, the structure elements should be larger than the size of the star and target

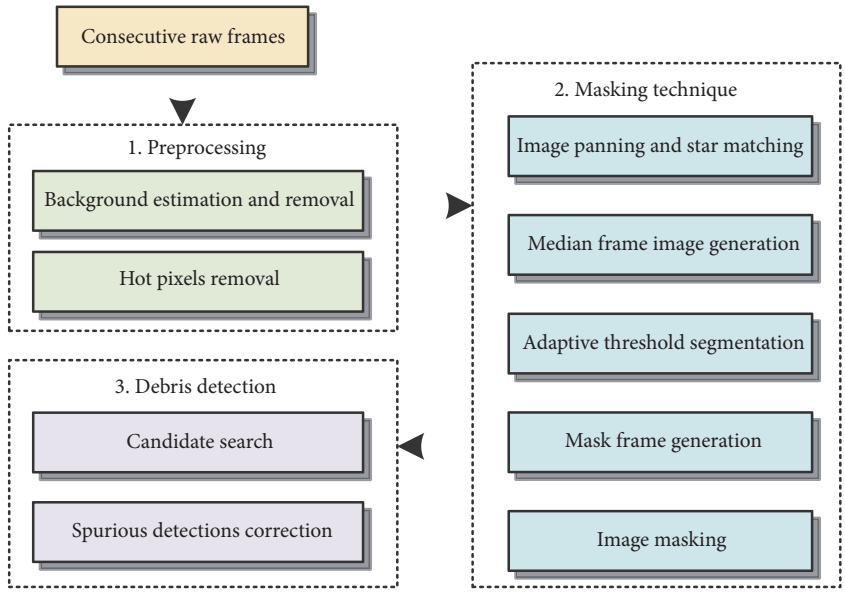


Figure 1: Block diagram of the proposed automatic pipeline.

in the field of view. Under the same observation mode of the same telescope, as long as the exposure time is constant, the structural elements remain unchanged. In this paper, the structure element is a $15 \times 15$ rectangle. The dilation operator $f \oplus b$ works as a maximal filter, while the erosion operator $f \ominus b$ works as a minimal filter. Based on these two operators, opening operator of gray image $f(i, j)$ by structure element $b(x, y)$ is defined as

$$(f \circ b) = (f \ominus b) \oplus b \tag{4}$$

The opening operator first makes an erosion operator and then makes the dilation operator. After transformation, the nonuniform background of image is estimated. Based on the opening operator, the TopHat transformation of a gray image is defined as

$$TH(f) = f - (f \ominus b) \oplus b \tag{5}$$

The TopHat transformation first makes an opening operator and then subtracts the operated image from the original image.

*2.2. Making Technique.* The detection technique is based on an algorithm comparing several consecutive frames of the same field in the sky. In these frames, objects are fixed and point-like. Conversely, the stars are stripe-like and move with fixed displacement. The so-called masking technique uses a mask frame to mask all background star on the search frames. The unmasked parts are then segmented for objects.

A mask frame is generated from several frames of the same field in the sky. In this paper, the stars were moved in consecutive frames. An image panning was needed to match stars in the same field. The mask frame was generated from a median frame of the panned frames since the median frame would only contain stars. The process is illustrated in Figure 2.

Three consecutive frames after image processing are described in Figure 2(a). The point-like object did not move during the three frames, while the stars were stripe-like and moved towards the upper right. According to the parameters of the telescope and information of image, the displacement of stars between two frames could be used for the calculation of image panning. Afterwards, the stars in the three proposed frames were in the same position. And the median frame of panned images would only contain stars. In this way, most parts of bright stars could be removed from the image sequences by the mask frame.

*2.3. Debris Detection.* Masking technique textcolorred removed the vast majority of stars in the image. It should be noted that stars may flicker in different images, as shown in Figure 3. And the median frame did not contain all the parts of the star, making the stars remain in the masked images.

The false alarm in this space debris detection mostly included star remnants, CCD noise, and cosmic rays, as shown in Figure 4(a). On basis of the masking technique mentioned in Section 2.2 the frames with candidate objects like Figure 4(e) were obtained. It could be clearly recognized that false alarms were not eliminated by the masking technique.

An appropriate segmentation algorithm was employed to remove the noise and get the appropriate candidate, as shown in Figure 4(f). The segmentation algorithm used in this paper was an adaptive segmentation method based on points constraints. The result of filtering is defined as follows:

$$f'(i, j) = \begin{cases} 1, & \text{if } f(i, j) \geq threshold; \\ 0, & \text{if } f(i, j) < threshold. \end{cases} \tag{6}$$

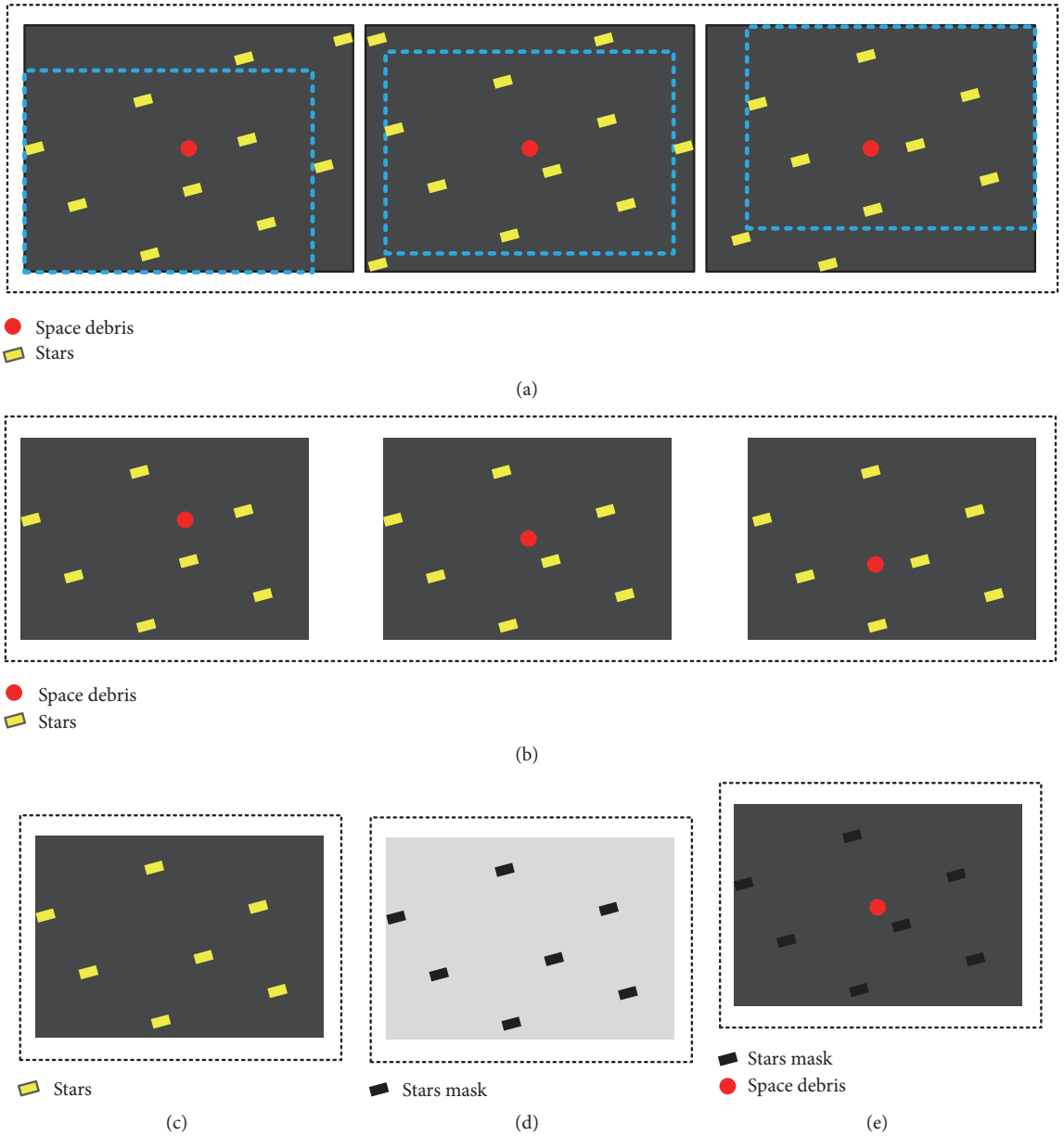


FIGURE 2: Masking technique illustrated by three frames taken at ground-based 600 mm telescope. (a) Three consecutive frames after image processing. (b) Image panning from (a). (c) The median frame of (b). (d) The mask image generated from (c). (e) An object is visible on the masked search frame. The frames are 1/100 part of the real frames taken by telescope.

where $f'(i, j)$ is the image after masking and panning, as shown in Figure 4(e). And threshold is set as

$$threshold = m + k\delta \tag{7}$$

where $m$ is the mean of background, $\delta$ is background standard deviation, and k is the coefficient determined by the number of points after segmentation.

A weighted algorithm was used to remove the false alarm and filter the correct candidate. Frames with candidate objects were generated by segmentation. And then, frames were panned to original position, as shown in Figures 4(f)-4(g). The weighted algorithm is defined as follows:

$$g(x, y) = \begin{cases} 1, & f_1'(i, j) + f_2'(x, y) + f_3'(x, y) \geq 2; \\ 0, & f_1'(i, j) + f_2'(x, y) + f_3'(x, y) < 2. \end{cases} \tag{8}$$

where $f_1'(i, j)$ is the pixel value of each point of the first frame and $f_2'(i, j)$ and $f_3'(i, j)$ are those of the second and last frames, respectively.

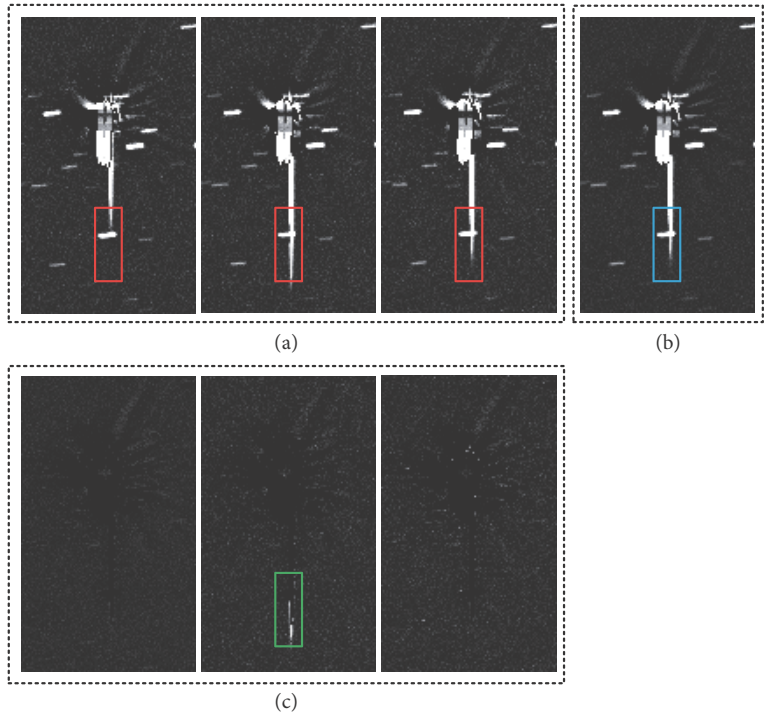


Figure 3: Bright stars flicker in different images. (a) Stars in three consecutive frames. (b) The median frame of (a). (c) The masked frames of (a).

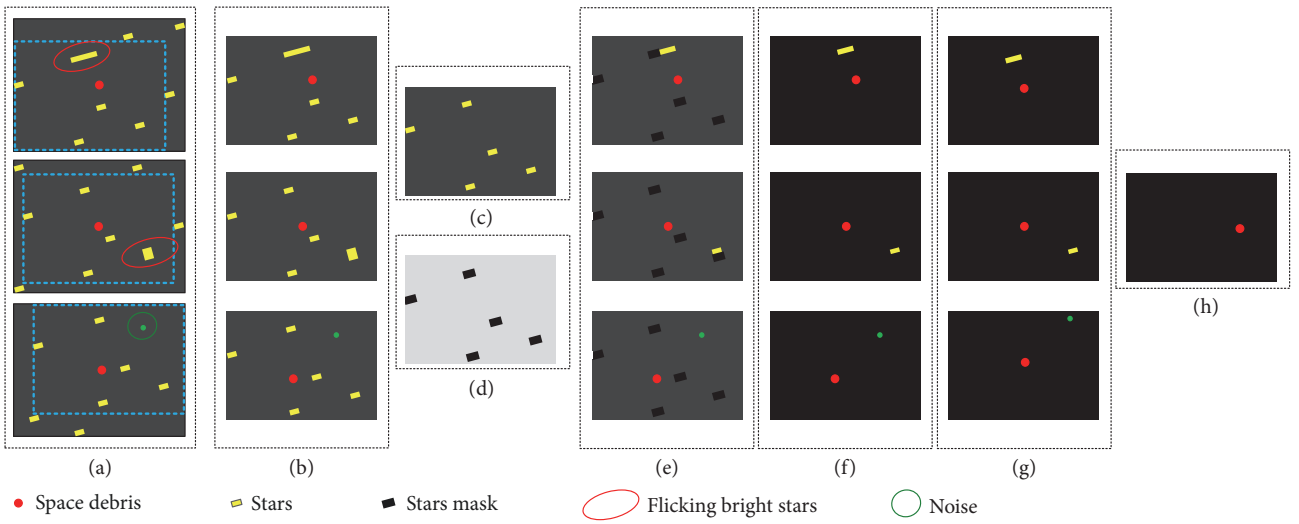


Figure 4: Step diagrams of image processing. (a) Consecutive raw frames with flicker stars and noise. (b) Frames panned to match stars. (c) Median frame of (b). (d) Mask frame. (e) Panned frames masked by mask frame. (f) Frames with candidate objects. (g) Frames panned to original position. (h) Frame after objects weighting.

## 3. Experiments and Disscussions

A 600 mm ground-based telescope is used in this survey. This telescope is dedicated to surveying space debris, and the parameters of the telescope are shown in Table 1. The telescope has a large field of view, resulting in a poor spatial resolution. The whole CCD frame is read out through only one channel, and the time interval between exposures is short enough for a high frame rate. The limiting V magnitude of the telescope is around 17 for an integration time of 3.6 s.

Consecutive raw frames with a space object were captured by the telescope, as shown in Figure 5(a). The exposure time for each frame is 1.4 s, and the raw frames textcolorred are 82 frames. There is only one GEO object in the space region,

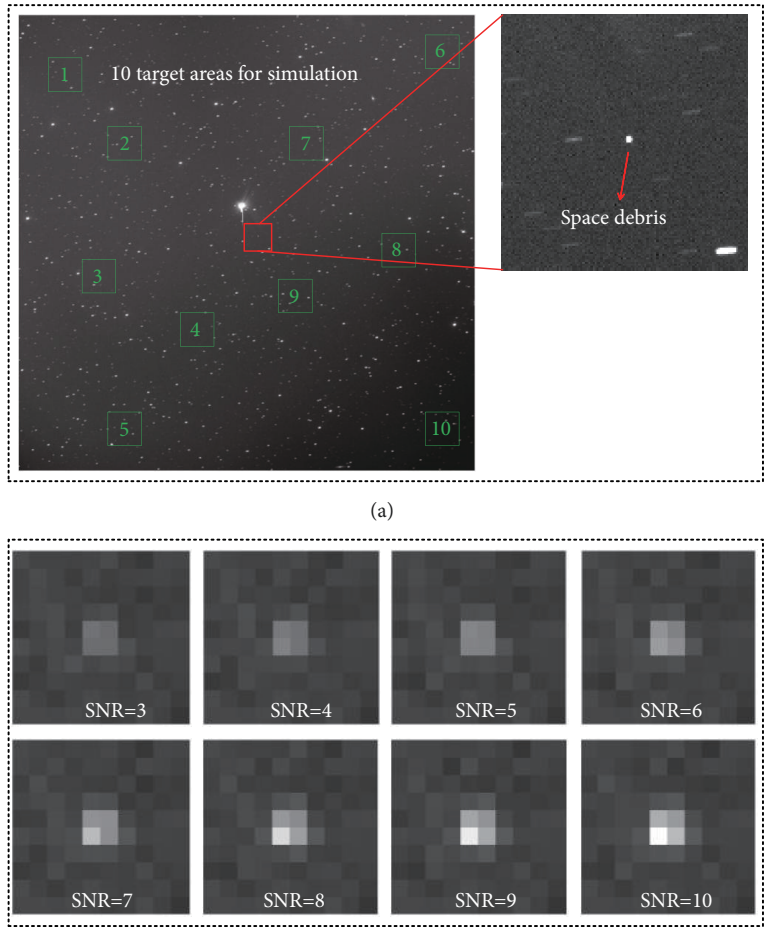


(a)

(b)

Figure 5: (a) A frame captured by the ground-based telescope. (b) Simulated pieces of space debris with different SNRs.

Table 1: Parameters of the telescope.

| Parameter | Value |
|---|---|
| Effective aperture of telescope | 680 mm |
| Focal length of telescope | 830 mm |
| Field of view | $3.3^\circ \times 3.3^\circ$ |
| Size of frame | $2040 \times 2040$ |
| Spatial resolution | $5.96''$ |
| Readout channels | 1 |

as shown in the blue box in Figure 5(a). In order to test the effect of the above algorithm of different SNR targets, ten areas are selected in the frame to add simulation targets, as shown in the green box in Figure 5(a). The purpose of adding simulation targets by selecting 10 fixed areas is to prevent the target from being different due to other problems, such as star occlusion and nonuniform background. The simulated pieces of space debris with different SNRs (from 3 to 10) were added to the star background images, as shown in Figure 5(b). The simulation target strictly follows the imaging characteristics of the space target taken by the telescope. The target size is $3 \times 3$ to $4 \times 4$, and 80% of the energy is concentrated in $2 \times 2$ pixels. Moreover, target energy satisfies the gaussian distribution in the spatial domain. The simulation target is directly superimposed on the star map, so that the gray level of the target in the sequence frame varies with the background fluctuation and noise. As much as possible to ensure that the simulation target and the actual target in the shape of the same.

Before the simulation of the space debris with different SNRs, the SNR is defined as follows:

$$SNR = \frac{\overrightarrow{s}}{\sigma_n} = \frac{s/N - m}{\sigma_n} \tag{9}$$

where $\overrightarrow{s}$ is the mean intensity of a piece of space debris, $\sigma_n$ is the standard deviation of the image noise, $s$ is the total intensity of the window area with a piece of space debris, $m$ is the mean of the image background, and $N$ is the number of pixels in the window.

The proposed algorithm was first performed on three frames of image for the evaluation of its performance in terms

Table 2: Detection probability and false-alarm rate of the masking technique.

| SNR | Total Number | Detected Number | Detection Probability (%) | False alarms | False alarm rate (%) |
|---|---|---|---|---|---|
| 3 | 800 | 758 | 94.75 | 16 | 2.00 |
| 4 | 800 | 765 | 95.63 | 12 | 1.50 |
| 5 | 800 | 772 | 96.50 | 8 | 1.00 |
| 6 | 800 | 778 | 97.25 | 5 | 0.63 |
| 7 | 800 | 783 | 97.88 | 3 | 0.38 |
| 8 | 800 | 787 | 98.37 | 1 | 0.13 |
| 9 | 800 | 791 | 98.88 | 1 | 0.13 |
| 10 | 800 | 792 | 99.00 | 1 | 0.13 |

Table 3: Parameters of frame raw.

| Field number | Analyzed CCD frames | Targets of total field |
|---|---|---|
| 112 | 112 × 8 | 248 |

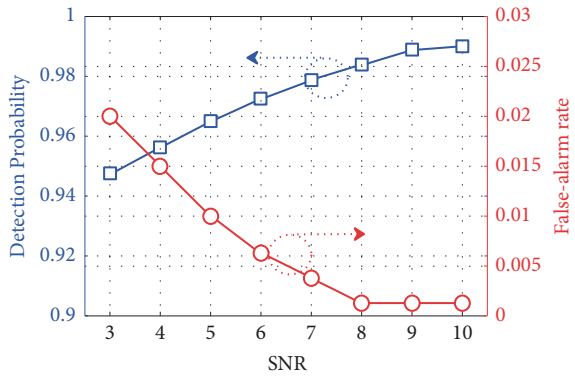


Figure 6: ROC curves of different SNRs.

of detection probability and false-alarm rate. They are given by

$$P_d = \frac{N_d}{N_{total}} \tag{10}$$

$$P_f = \frac{N_f}{N_{total}} \tag{11}$$

where $P_d$ is the detection probability, $P_f$ is the false-alarm rate, and $N_d$, $N_f$, and $N_{total}$ are the numbers of detected space debris, false-alarms, and total space debris in the image sequence, respectively.

There are 82 frames in total. And only three frames are required for targets extraction, so the image can be tested at 80 times. There are 10 simulation targets in each frame, so the total number of targets is 800. The test results of masking technique are shown in Table 2 and Figure 6. And the receiver operating characteristic (ROC) results for the three images masking technique are shown in Figure 7. The masking technique can successfully detect 99.00% of the space debris with SNRs as low as 10. The detection probability is 99.00%, and the false-alarm rate is 0.13%. When the SNR equals 3, the detection probability of the proposed technique can still reach 94.75% with the false alarm rate of 2.00%. As shown

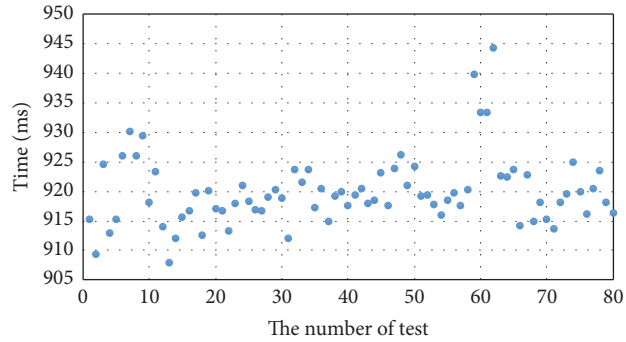


Figure 7: Time cost of the algorithm.

in Table 2, the higher the SNR is, the better the masking technique performs. The only space debris in Figure 5(a) has a SNR of up to 45.35, and 80 experiments have been carried out in the sequence frame. The results show that the detection rate is as high as 100% and the false alarm rate is 0.

When the image size is 2040 × 2040, and three frames are used for space target detection, the algorithm running time is shown in Figure 7. Totally 80 algorithm tests were carried out using the image sequence taken by the 600 mm telescope. The experimental results showed that the average operation time of the algorithm was 920 ms, among which the longest was 944 ms and the shortest 908 ms. The operation time is kept within 1.4 s to ensure the engineering demand.

To investigate the efficiency of masking technique, the image frames of different field in the sky were tested. The parameter of frame raw of GEO region is shown in Table 3. There are 112 space fields tested by the proposed technique. Eight frames of each field are analyzed, in order to make sure the detection probability and false-alarm rate. Total targets of the 112 GEO field are 248. The total number of this survey is 248 × 6, because the number of each field is eight, which provides six tests for our detection. Test results of GEO space debris detection are shown in Table 4. The detection probability of this survey is 95.90%, with the false-alarm rate of 0.34%.

## 4. Conclusions

A method is presented in this paper for the detection of space debris in GEO orbits. The background of space debris

Table 4: Etection probability and false-alarm rate of the masking technique.

| Total Number | Detected Number | Detection Probability (%) | False alarms | False alarm rate (%) |
|---|---|---|---|---|
| $248 \times 6$ | 1427 | 95.90 | 5 | 0.34 |

includes thin cloud in the sky and light condition as well as different CCD channels. Image preprocessing is applied to the estimation and removal of nonuniform background. Under the background, there are a large number of stars that have nearly the same intensity distribution as the space debris. Therefore, a masking technique of star removal is critical to space debris detection and false alarm rejection. Besides, a weighted algorithm is adopted in object detection so as to remove the false alarm and filter the correct candidate. The algorithm was tested on a 600 mm telescope in Lijiang, China. Simulation targets with SNR of 3 to 10 are added to the sequence frame images taken by the telescope to test the extraction effect of the algorithm for targets with different SNR. In addition, the algorithm is also used to extract space objects in multiple sky regions in GEO region. According to the experimental results, the proposed image preprocessing and masking technique can effectively reject false alarms and exhibits a high detection probability with only three frames.

## Data Availability

The data used to support the findings of this study are available from the corresponding author upon request.

## Conflicts of Interest

The authors declare that they have no conflicts of interest.

## Acknowledgments

The research is supported by National Natural Science Foundation (NSFC) of China under project No. 60978050.

## References

[1] T. Schildknecht, "Optical surveys for space debris," *The Astronomy and Astrophysics Review*, vol. 14, no. 1, pp. 41–111, 2007.

[2] R.-Y. Sun, J.-W. Zhan, C.-Y. Zhao, and X.-X. Zhang, "Algorithms and applications for detecting faint space debris in GEO," *Acta Astronautica*, vol. 110, pp. 9–17, 2015.

[3] N. C. Mohanty, "Computer tracking of moving point targets in space," *IEEE Transactions on Pattern Analysis and Machine Intelligence*, vol. 3, no. 5, pp. 606–611, 1981.

[4] I. S. Reed, R. M. Gagliardi, and H. M. Shao, "Application of three-dimensional filtering to moving target detection," *IEEE Transactions on Aerospace and Electronic Systems*, vol. 19, no. 6, pp. 898–905, 1983.

[5] D. Zhang, K. Wang, J. Yi, B. Peng, and J. Tan, "Application of three-dimensional filtering to moving target detection," in *Proceedings of the IEEE International Conference on Signal Processing*, 2017.

[6] I. S. Reed, R. M. Gagliardi, and L. B. Stotts, "A recursive moving-target-indication algorithm for optical image sequences," *IEEE Transactions on Aerospace and Electronic Systems*, vol. 26, no. 3, pp. 434–440, 1990.

[7] Y. Barniv, "Dynamic programming solution for detecting dim moving targets," *IEEE Transactions on Aerospace and Electronic Systems*, vol. 21, no. 1, pp. 144–156, 1985.

[8] S. Buzzi, M. Lops, and L. Venturino, "Track-before-detect procedures for early detection of moving target from airborne radars," *IEEE Transactions on Aerospace and Electronic Systems*, vol. 41, no. 3, pp. 937–954, 2005.

[9] M. Wei, N. H. Chen, Y. T. Yan, Z. Q. Wu, and B. Xu, "The detecting methods of geostationary orbit objects," in *Proceedings of the 3rd International Symposium on Intelligent Information Technology and Security Informatics*, IEEE Computer Society, 2010.

[10] J. Silha, T. Schildknecht, A. Hinze, T. Flohrer, and A. Vananti, "An optical survey for space debris on highly eccentric and inclined MEO orbits," *Advances in Space Research*, vol. 59, no. 1, pp. 181–192, 2017.

[11] T. Schildknecht, R. Musci, M. Ploner et al., "Optical observations of space debris in GEO and in highly-eccentric orbits," *Advances in Space Research*, vol. 34, no. 5, pp. 901–911, 2004.

[12] T. Schildknecht, U. Hugentobler, and M. Ploner, "Optical surveys of space debris in GEO," *Advances in Space Research*, vol. 23, no. 1, pp. 45–54, 1999.

[13] T. Schildknecht, U. Hugentobler, and A. Verdun, "Algorithms for ground based optical detection of space debris," *Advances in Space Research*, vol. 16, no. 11, pp. 47–50, 1995.

[14] R.-Y. Sun and C.-Y. Zhao, "A new source extraction algorithm for optical space debris observation," *Research in Astronomy and Astrophysics*, vol. 13, no. 5, pp. 604–614, 2013.

[15] J. Xi, D. Wen, O. K. Ersoy et al., "Space debris detection in optical image sequences," *Applied Optics*, vol. 55, no. 28, pp. 7929–7940, 2016.